



HAL
open science

Demonstrating the Potential of Low-Cost GNSS Receiver for tidal monitoring, storms, and flood detecting: example of 2022 Noru Storm in Thua Thien Hue province, Vietnam

Phuong Lan Vu, Minh Cuong, Phuong Bac Nguyen, Huu Duy Nguyen, Thi Bao, Hoa Dinh, Thuy Hang Nguyen, Gheorghe Şerban, Martina Zelenakova, José Darrozes

► **To cite this version:**

Phuong Lan Vu, Minh Cuong, Phuong Bac Nguyen, Huu Duy Nguyen, Thi Bao, et al.. Demonstrating the Potential of Low-Cost GNSS Receiver for tidal monitoring, storms, and flood detecting: example of 2022 Noru Storm in Thua Thien Hue province, Vietnam. *Acta Montanistica Slovaca*, 2023, 28 (4), pp.1034-1046. 10.46544/ams.v28i4.19 . hal-04921103

HAL Id: hal-04921103

<https://ut3-toulouseinp.hal.science/hal-04921103v1>

Submitted on 30 Jan 2025

HAL is a multi-disciplinary open access archive for the deposit and dissemination of scientific research documents, whether they are published or not. The documents may come from teaching and research institutions in France or abroad, or from public or private research centers.

L'archive ouverte pluridisciplinaire **HAL**, est destinée au dépôt et à la diffusion de documents scientifiques de niveau recherche, publiés ou non, émanant des établissements d'enseignement et de recherche français ou étrangers, des laboratoires publics ou privés.



Distributed under a Creative Commons Attribution 4.0 International License

Demonstrating the Potential of Low-Cost GNSS Receiver for tidal monitoring, storms, and flood detecting: example of 2022 Noru Storm in Thua Thien Hue province, Vietnam

Phuong Lan Vu¹, Minh Cuong Ha², Phuong Bac Nguyen¹, Huu Duy Nguyen¹,
Thi Bao Hoa Dinh¹, Thuy Hang Nguyen³, Gheorghe Șerban^{4*}, Martina Zelenakova⁵
and José Darrozes⁶

Authors' affiliations and addresses:

¹ VNU - University of Science, 334 Nguyen Trai Str. Hanoi, Vietnam

e-mail: yuphuonglan@hus.edu.vn;

nguyenhuuduy@hus.edu.vn;

dinhthibaohoa@hus.edu.vn;

Phuongbac.nguyen.1801@gmail.com;

² VNU - University of Engineering and Technology, 144 Xuan Thuy str. Hanoi, Vietnam.

e-mail: cuonghm@vnu.edu.vn

³ VNU - Vietnam Japan University (VJU), Vietnam National University (VNU), Hanoi, Vietnam, e-mail:

ntt.hang2@vju.ac.vn

^{4*} Faculty of Geography, Babes-Bolyai University, Cluj-Napoca, Romania e-mail:

gheorghe.serban@ubbcluj.ro

⁵ Department of Environmental Engineering, Faculty of Civil Engineering, Technical University of Kosice, Slovakia

e-mail: martina.zelenakova@tuke.sk

⁶ Géosciences Environnement Toulouse (UMR 5563 CNRS), 14 avenue Edouard Belin, 31400 Toulouse, France, e-mail: jose.darrozes@get.omp.eu

*Correspondence:

Gheorghe ȘERBAN, Faculty of Geography, Babes-Bolyai University, Cluj-Napoca.

tel.: +84 9 14 35 97 81

e-mail: gheorghe.serban@ubbcluj.ro

Funding information:

Vietnam National Foundation for Science and Technology Development (NAFOSTED) project number 105.08-2020.17

How to cite this article:

Phuong Lan Vu¹, Minh Cuong Ha², Phuong Bac Nguyen¹, Huu Duy Nguyen¹, Thi Bao Hoa Dinh¹, Thuy Hang Nguyen³, Gheorghe Șerban^{4*}, Martina Zelenakova⁵ and José Darrozes (2023). Modular wind generators for autonomous power supply to remote mining areas mineral resources. *Acta Montanistica Slovaca*, Volume 28 (4), 1034-1046

DOI:

<https://doi.org/10.46544/AMS.v28i4.19>

Abstract

Extreme hydrological events such as tsunamis, high tides, or storm surges seriously threaten coastal communities. These events result in flooding, property damage, loss of life, and long-term economic and social impacts. Therefore, monitoring and detecting extreme hydrological events significantly affect coastal areas in disaster response efforts. However, the cost of installing and maintaining these stations can be a significant challenge for developing countries. The objective of this study is to use a low-cost GNSS receiver to monitor tides and detect extreme coastal hydrological phenomena by analyzing changes in water level, using analysis of the signal-to-noise ratio (SNR) data. Data used in this study were collected from a GNSS station located in the Tam Giang Lagoon area, Thua Thien Hue, Vietnam, from September to October 2022. The water level based on GNSS-R is compared with the sensor's measured water level, with the Pearson correlation coefficient reaching 0.96 and RMSE of 0.08m. Continuous Wavelet Transform analysis demonstrated the relationship between water levels and extreme hydrological events. The results show that distinct signatures in the data correspond to the Noru typhoon from September 27-29, 2022, and the inundation from October 14-19, 2022, in Thua Thien Hue. This information is the basis for forecasting and early warning of extreme events and informing disaster response and management efforts.

Keywords: Extreme hydrological events, GNSS-R, Interference Pattern Technique (IPT), Singular Spectrum Analysis (SSA), Continuous Wavelet Transform (CWT).



© 2023 by the authors. Submitted for possible open access publication under the terms and conditions of the Creative Commons Attribution (CC BY) license (<http://creativecommons.org/licenses/by/4.0/>).

Introduction

Climate change has increased extreme weather events, including heatwaves, droughts, floods, and hurricanes, resulting in billions of dollars worth of disasters each year globally (Seneviratne, 2021; S Jonas, 2018; Malhi GS, 2021; Mohammad Kazemi Garajeh, 2023). According to the World Meteorological Organization (WMO), over the past 50 years, extreme climate events have resulted in an average of 115 deaths and \$202 million in damages per day. The number of disasters has increased fivefold in the past 50 years due to the effects of climate change (World Meteorological Organization, 2021). Extreme hydrological events account for 50% of total disasters, especially storms and floods. Economic damage caused by storms accounts for about 521 billion USD, and floods account for about 115 billion USD. Hurricanes are the most common cause of damage, leading to the greatest economic losses globally (Jérôme Benveniste et al., 2019) and directly affecting coastal communities (Kaitano Dube, 2022; Ben Clarke, 2022; Lukas Gudmundsson et al., 2021; Tabari, 2022). Different responses do not always work best for coastal communities. Therefore, monitoring techniques have been developed to accurately identify and predict extreme hydrological events in order to provide warnings and assess their impacts (Prashant Kumar et al., 2021; Jonathan M. Frame, 2022; Kovanič et al., 2024). In particular, monitoring and measuring water levels is an important information channel in identifying and assessing coastal hazards (Tasneem Ahmed, 2023; Vousdoukas et al., 2018; Benveniste et al., 2019). This information can be used to develop early warning systems, inform emergency planning and response efforts, and support long-term adaptation and mitigation strategies.

Currently, water level monitoring is done using a range of techniques, including tide gauges, buoys (Heiko Apel, 2012), and satellite-based measurements (Phuong Lan Vu et al., 2018; Haas, 2014; Crétaux, 2017; S. Biancamaria et al., 2017; Arjumand Z. Zaidi et al., 2021; Jieying Lao, 2022; Kovanič et al., 2023a). Some of the global tidal measuring systems can be mentioned as the Global Sea Level Observing System GLOSS (<https://www.sonel.org>) or the US National Water Level Observation Network NWLON (<https://tidesandcurrents.noaa.gov/>). Although these stations allow continuous measurement, they are limited in space and have high operating costs. Satellite radar altimeters have proven their feasibility in monitoring sea levels and observing high tides or storm surges (Xiaohui Li, 2018; Ole B. Andersen, 2015; Charls Antony, 2014; Tao Ji, 2019; Cazenave R. J., 2010; Zhou Qiu, 2019). However, the limitations of satellite altimetry are the low spatial/temporal resolution and many disadvantages when studying coastal waters due to the influence of the land. In addition, the wavelength resolution of altimetry data is limited by the sampling interval, making it difficult to accurately observe sea level (Cazenave A., 2018) in coastal areas. This means that small-scale ocean features, such as eddies, currents, etc., may not be captured in detail, and their dynamics may be poorly understood.

In recent years, a coastal global navigation satellite system (GNSS) network has been developed to monitor water level changes by recording signals reflection from the sea surface (K. M. Larson et al., 2020; N. Roussel et al., 2015; J. Beckheinrich et al., 2014; Frédéric Frappart, 2016; N. Roussel et al., 2015), also known as GNSS reflectometry (GNSS-R). The results show that GNSS-R can achieve similar or higher accuracy than traditional water level measurement methods (Xiaolei Wang, 2021; D. Purnell et al., 2020; Haas, 2014). In addition, GNSS-R data is also used to detect extreme hydrological events such as storm surges and floods. Some research works can be mentioned as Phuong Lan Vu et al. (Phuong Lan Vu et al., 2019) analyzed GNSS-R data obtained at the GNSS geodetic station in Socoa, France, to determine the tidal components and identify the 2010 Xynthia storm signature. Su-Kyung Kim et al. (Su-Kyung Kim et al., 2021a; Su-Kyung Kim, 2021b) have successfully detected the extreme change in water level caused by coastal hazards using the water level recovery method based on GNSS-R data. The proposed method has been confirmed by extreme events such as the 2012 Haida Gwaii earthquake, the 2015 Chilean earthquake, and the storm surge caused by Hurricane Harvey in 2017. Dongju Peng et al. (Dongju Peng, 2019) used the GNSS reflected signal to detect extreme sea level variations caused by weather, specifically the Hato storm in 2017 and the Mangkhut storm in 2018 in Hong Kong. The results of this study demonstrate that GNSS reflectometry provides a new approach to storm surge monitoring and complements existing tidal measuring networks. Xiaohui Li (Xiaohui Li et al., 2021) reconstructed wind fields by combining coastal GNSS-R winds with ECMWF winds to create a storm surge model off the coast of China during Typhoon Utor 2013. The study demonstrated that the coastal GNSS-R wind impacts the accuracy of storm surge determination and indirect forecasting by improving initial conditions. Wentao Yang et al. used GNSS-R (CYGNSS Level 1 Science Data products) observations to detect and map floods in the catastrophic July 2021 flooding in Henan province, China (Wentao Yang, 2021). The results demonstrated that GNSS-R data with high spatial and temporal resolution is capable of rapid flood monitoring and flood area mapping. However, the high cost of installing a standard GNSS-R station has limited its wider application, especially in poor countries and in adverse weather conditions.

Recently, low-cost GNSS antennas have been used for water level monitoring (Phuong Lan, 2022; M. A. R. Fagundes, 2021) and monitoring coastal hazards (Tasneem Ahmed, 2023; Kovanič et al., 2023b); the obtained results have demonstrated that low-cost GNSS is more suitable than standard geodetic antennas because the geodetic standard antennas are designed to reduce multipath signals (the signal is used to retrieve water level). Purnell et al. (David J. Purnell, 2021; Kovanič et al., 2021; Kovanič et al., 2022) used multiple low-cost multi-

frequency GNSS antennas co-located to eliminate the effect of random noise in the SNR (Signal-to-Noise Ratio) signal and improve the accuracy of the water level measurement with costs only a fraction of the cost of a standard geodetic antenna. Chenyu Xue et al. (Chenyu Xue, 2022) evaluated the accuracy of low-cost multi-GNSS receivers in motion monitoring and developed methods using a low-cost dual GNSS receiver system of proximity to enhance their high performance.

This study aims to demonstrate the feasibility of low-cost multi-frequency GNSS stations in detecting and predicting extreme hydrological events. GNSS-R data were obtained during the period of the Noru Typhoon in September 2022, and the flood occurred in late October 2022 in Thua Thien Hue province, Vietnam. This is also the first time that a low-cost GNSS-R receiver, i.e., Alpha Polaris, has been used to study coastal hazards in Vietnam.

Study area and datasets

Study area

The study area is Tam Giang Lagoon (Fig. 1), extending from the mouth of O Lau River to Thuan An Bridge with a length of 25 km, and belongs to the Tam Giang - Cau Hai lagoon system in the Thua Thien Hue province (Fig. 1a). Tam Giang lagoon's width (fig. 1b) varies from 0.5 to 4km (My Thanh, Quang Dien), averaging nearly 2.5km, and has a depth ranging from 2 to 7 m, with creeks up to 10 m deep (Duc Thanh Tran et al., 2022). The climate is divided into two distinct seasons: The dry season, from March to August, is influenced by the southwest wind, so the air is hot and dry (Fig. 2). The rainy season is from September to January of the next year, and storms usually appear around September to October. Due to its location at the intersection of several rivers, the lagoon experiences strong currents, large waves, and strong winds, which can create dangerous whirlpools. So, the Tam Giang Lagoon is often directly affected by floods and storms that hit Thua Thien Hue province. According to statistical data in 2021, from 1952 to 2020, 47 storms and tropical depressions directly affected Thua Thien Hue province, with an average of 4-5 floods per year, causing much damage to people and property. Typhoon Noru made landfall in Thua Thien Hue on the night of September 27, 2022, with winds of up to 133km/h and widespread heavy rain, one of the strongest storms to hit Vietnam in the past two decades. Typhoon Noru left 3 people dead and missing, more than 7,000 houses were flooded, and causing damage of more than 50 million dollars in Thua Thien Hue.

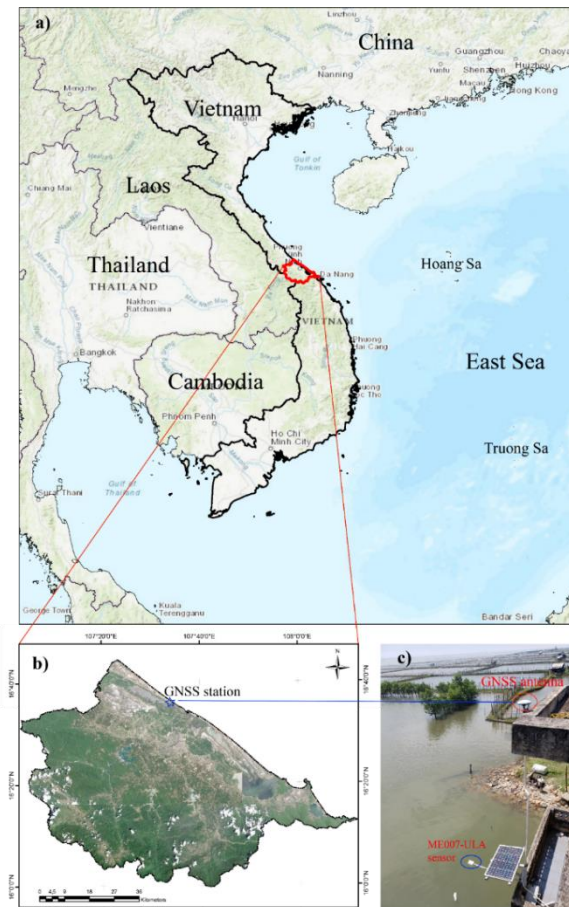


Fig. 1. a) Study area in Hue province in Vietnam; b) The location of GNSS station in Tam Giang lagoon, Thua Thien Hue province. c) GNSS antenna at 8.3m above sea level and co-located meteorological sensor marked as red and blue circles, respectively

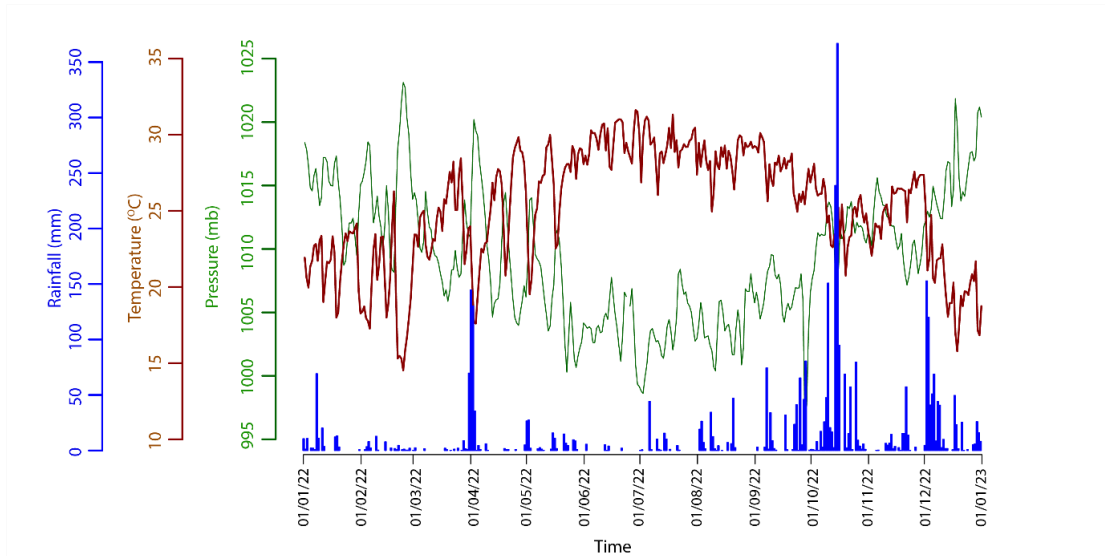


Fig. 2. Rainfall (blue), temperature (brown), and pressure (green) data are also collected at the Hue meteorological station about 20km from the GNSS station.

Datasets

- **Experiment setup:** The GNSS station is installed in Tam Giang lagoon at coordinates 16°35'47.8"N, 107°34'05.3"E, and an elevation of 8.3m above sea level. The antenna is installed at a height of 8.3 m above sea level (Fig. 1c). GNSS data was collected from September to October 2022 at 1Hz frequency. The equipment used is a low-cost Alpha+30 Polaris GNSS receiver (the cost is only \$399), which can receive bi-frequency signals of all existing GNSS constellations (GPS (USA), GLONASS (Russia), Galileo (Europe), Compass/Beidou (China), two regional navigation systems IRNSS (India), QZSS (Japan), and in development CAGAN (Indian) or BDSBAS (China) Satellite-based Augmentation Systems (SBAS. The GNSS Alpha Polaris allows the reception of up to 230 channels in one or both L1 and L2 bands with relatively high accuracy. In addition, the device also consumes a low power supply of 5V, saving energy with an update rate ranging from 1Hz to 20Hz.

- **In-situ data:** The reference water level data was recorded at the same time as the GNSS-R data, which is based on the sonar distance measurement technique using the ME007-ULA module installed at the GNSS-R station. This module is dustproof, waterproof, and suitable for long-term continuous measurement in coastal environments. The ME007-ULA measures at 40KHz, and the accuracy in UART Output mode is about ± 20 mm and is converted to the GPS standard time (Timestamp).

- **Meteorological data:** Meteorological data is recorded from the BME280 sensor once every second (Fig. 1c). Outliers in raw data are removed before they are grouped and summarized into one-hour resolution. The barometer inversion method is used to convert atmospheric pressure to sea level using the following equation (Ponte, 2006):

$$h_a = - \frac{P_a - \bar{P}_a}{\rho g_n} \tag{1}$$

where P_a is the atmospheric pressure time series, $\rho = 1.020 \text{ gm/cm}^3$ is the reference ocean density and g_n is the mean acceleration due to gravity. The value of g_n varies depending on the latitude and altitude of the location on the Earth's surface and is calculated by the formula:

$$g_n = 978.03185(1.0 + 0.005278895 \sin^2\Phi - 0.000023462 \sin^4\Phi) \quad (\text{cm/s}^2)$$

where Φ is the latitude of the study area. In this study, the $g_n = 9.78\text{ms}^{-2}$.

Methods

Figure 3 shows the main steps in GNSS data processing to obtain the GNSS-based height of the sea surface (SSH) with respect to the reference ellipsoid, i.e., WGS84.

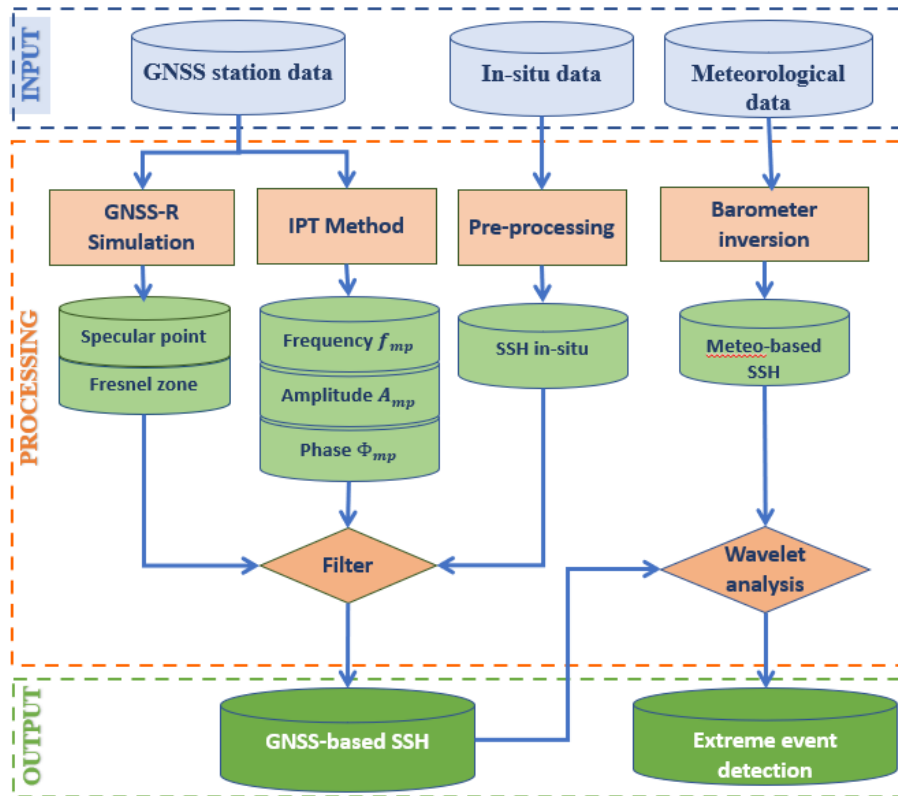


Fig. 3. Methodology processes.

GNSS-R simulation

The simulation of the GNSS ray tracing is based on determining the position of the reflector points when the coordinates of the receiver and satellite are known (N. Roussel, 2014). GNSS-R simulation is developed using the R programming language with the input data of the receiver coordinates, the satellite ephemeris, and a set of optional environmental parameters to eliminate reflections that are not in the water area. Satellite coordinate information is obtained from NASA's Archive of Space Geodesy Data (CDDIS) in SP3 format; these products are available at: <https://cddis.nasa.gov/archive/gnss/products/>. The simulation results are the time-based reflection point coordinates and Fresnel zone. In this study, to avoid the reflection areas from the ground, an azimuth mask, and a satellite high-angle mask were used for the simulation results.

Inverse modeling of SNR data using the IPT method to retrieve the water level time series

The Interference modeling technique (IPT) is based on analyzing multipath signals appearing in GNSS SNR data continuously recorded by GNSS receivers (Nicolas Roussel, 2015; J. S. Löfgren, 2011). In which the SNR values save the constructive interference between the direct signal and the reflected signal (Fig. 4). The SNR signals were recorded on the different frequencies of GNSS (i.e., L1, L2, and L5 for GPS constellation; E1, E2, E5 for Galileo and so on). These signals create oscillations due to multipath, and the frequency is calculated by the following function (Kristine M. Larson, 2008):

$$\tilde{f} = \frac{4\pi}{\lambda} \left(\dot{h} \frac{\tan(\theta)}{\dot{\theta}} + h \right) \tag{2}$$

where \tilde{f} is the frequency of the multipath oscillation, h the distance between the antenna phase center and the reflecting surface, λ is the wavelength of the signal, θ the satellite elevation angle, $\dot{h} = dh/dt$ is the vertical velocity of the reflecting surface, and $\dot{\theta} = d\theta/dt$ is the elevation angle velocity.

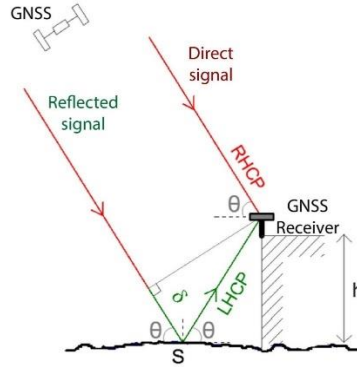


Fig. 4. Principle of a GNSS reflectometer with a single antenna.

Equation 2 shows that if we consider a reflecting surface to be static ($\dot{h} \approx 0$), then \tilde{f} is constant and proportional to the height of the antenna. In the dynamic case $\dot{h} \neq 0$ (due to waves, tides, storms), \tilde{f} then depends on satellite elevation angle θ , its rate of change $\dot{\theta}$ and its altitude change rate reflecting surface \dot{h} . Then, equation 2 has two unknowns: h and \dot{h} . To eliminate the parabolic effects of the direct signal on the SNR records, the multipath residual SNR_m is used to calculate the height of the water level (J. S. Löfgren, 2011):

$$SNR_m = A \cos\left(\frac{4\pi h}{\lambda} \sin(\varepsilon) + \psi_m\right) \tag{3}$$

where A is the amplitude, λ is the wavelength, and ψ_m is the phase difference between direct and reflected signals.

Analysis of GNSS-R for storm surge detection

Singular spectrum analysis - SSA

The single spectrum analysis (SSA) technique developed in time series analysis is applied in many fields, such as multivariate statistics and digital signal processing (R.Vautard and M.Ghil, 1989). The SSA method collects and analyzes a spectrum of single values to identify and distinguish between signal and noise in a given time series. This process consists of two main stages:

Stage 1- Singular Value Decomposition (SVD) consists of two steps:

If we consider a signal $\{X_{(t)}: t = 1, \dots, N\}$ of length N and let M be an integer called the window length. We embedded the original time series into a vector space of dimension M by forming X_i lagged vectors (the columns of the matrix \mathbf{X}). The elements (c_j) of this matrix are determined by the formula:

$$c_j = \frac{1}{N-j} \sum_{i=1}^{N-j} x(t_i) x(t_{i+1}) \quad \text{with } 0 \leq j \leq M - 1$$

where t_i and t_{i+1} are the sampling times.

Constructing a matrix $\mathbf{S} = \mathbf{C}\mathbf{C}^T$ to apply SVD and denote λ_k the eigenvalues of \mathbf{S} taken in the decreasing order of magnitude and E_j^k the eigenvectors of the matrix \mathbf{S} corresponding to these eigenvalues λ_k .

Following Vautard and Ghil (R.Vautard and M.Ghil, 1989), the SVD of the matrix \mathbf{X} can be follows as $\mathbf{X} = X_1 + \dots + X_k$

where the k^{th} principal components among M is given by:

$$a^k(t_i) = \sum_{j=1}^M x(t_{i+j}) E_j^k \quad \text{with } 0 \leq i \leq N - M$$

Stage 2- Reconstruction consists of two steps, namely i) grouping and ii) averaging diagonally for the purpose of signal and noise discrimination. The components of the original time series analyzed using SSA are reconstructed as follows:

$$x^k(t_i) = \frac{1}{M} \sum_{j=1}^M a(t_{i-j}) E_j^k \quad \text{with } M \leq i \leq N - M + 1$$

where $x^k(t_i)$ is the k^{th} reconstructed components (RC_k) of the original times series.

CWT – Continuous Wavelet Transform

Continuous Wavelet Transform (CWT) decomposes a function into sinusoids of different frequencies to remove noise from signals and identify the raw signal's main components and associated scale. The CWT is defined

as the sum over all time of the signal multiplied by scaled and shifted versions of the wavelet mother function (Box & Jenkins, 1970):

$$C_x(a, \tau) = \int_{-\infty}^{+\infty} x(t) \psi_{a,\tau}^* dt ; \psi_{a,\tau}(t) = \frac{1}{a} \psi\left(\frac{t-\tau}{a}\right) \quad (4)$$

where $x(t)$ is the signal in the time domain, * denotes the complex conjugate, and $\psi(t)$ is the mother wavelet scaled by a factor a , $a > 0$, and dilated by a factor τ . In the CWT, the time and scale parameters (a , τ) are continuous. The result of the CWT is a map of wavelet coefficients $C_x(a, \tau)$. Afterward, a wavelet spectrum $W_x(a, \tau)$ is constructed according to the relation below, defined as the modulus of the wavelet coefficients (Torrence & Compo, 1998):

$$W_x(a, \tau) = C_x(a, \tau) C_x^*(a, \tau) = |C_x(a, \tau)|^2 \quad (5)$$

The advantages of CWT in the tidal analysis are (1) more accurate results for periods with fluctuating tidal characteristics and (2) better temporal resolution for changes in frequency. In addition, the CWT analyses is used to remove the tidal components in favor of analysis of other physical characteristics of the signal, i.e., surge, inverse barometer (IB) effect, and so on.

Results

Water level determination results and validation

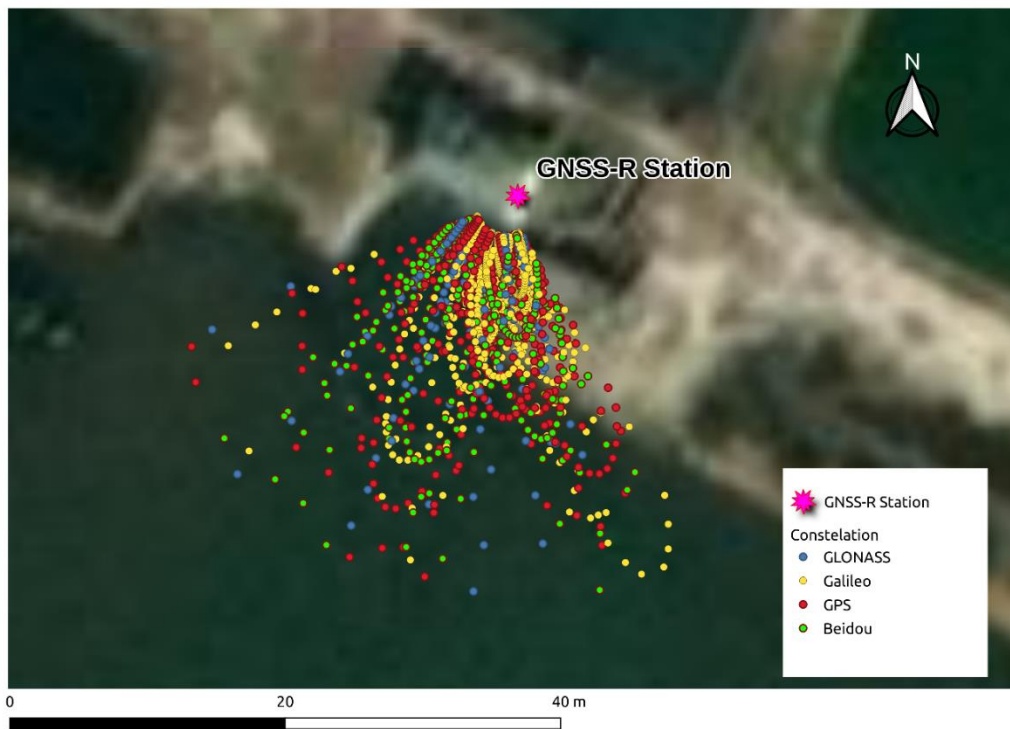


Fig. 5. Location of the Specular Reflection Point with GNSS constellations in the study area for one day: 02/09/2022 (31 GPS, 18 GLONASS, 25 GALILEO, 34 BEIDOU satellites)

GNSS-R data is processed through a simulation step to eliminate reflections that are not on the water surface ground, building, bridge, vegetation, etc.) by using elevation angles in the range of 2 to 25 degrees and azimuth masks from 150 to 250 degrees (Fig. 5). The IPT method is applied to estimate water level variation over time for all satellites observed in the study area. Figure 5 shows the results of the water level time series based on each satellite constellation with a slide window interval of 5 minutes. Table 1 shows the comparison results between the water level based on GNSS-R and the water height measured by the sensor through metrics: root mean square error (RMSE), number of measurements (N), bias, and correlation coefficient (R) to evaluate the accuracy of the SSH derived from different satellite constellations. The raw results showed that the different satellite constellations provide similar accuracy when estimating water levels, with an RMSE of 0.08m and a correlation coefficient of 0.96. Figure 5 shows many outliers that are independent of the constellation and artificially increase this RMSE.

If we now apply an outlier filter, we can see that the RMSE strongly decreases, and the red curve (Fig. 6) is much smoother and better reflects the true variability of the SSH time series.

Tab. 1. Comparisons between GNSS-based SSH and in-situ SSH in Tam Giang lagoon, Thua Thien Hue (Number of observations N , root mean square error RMSE, Bias and the correlation coefficient R)

Constellations	R	RMSE (m)	Bias	Number of observations (N)
GPS	0.97	0.06	0.008	210
GLONASS	0.96	0.06	0.009	84
GALILEO	0.96	0.05	0.006	202
BeiDOU	0.97	0.06	0.003	54
All	0.96	0.05	0.010	274

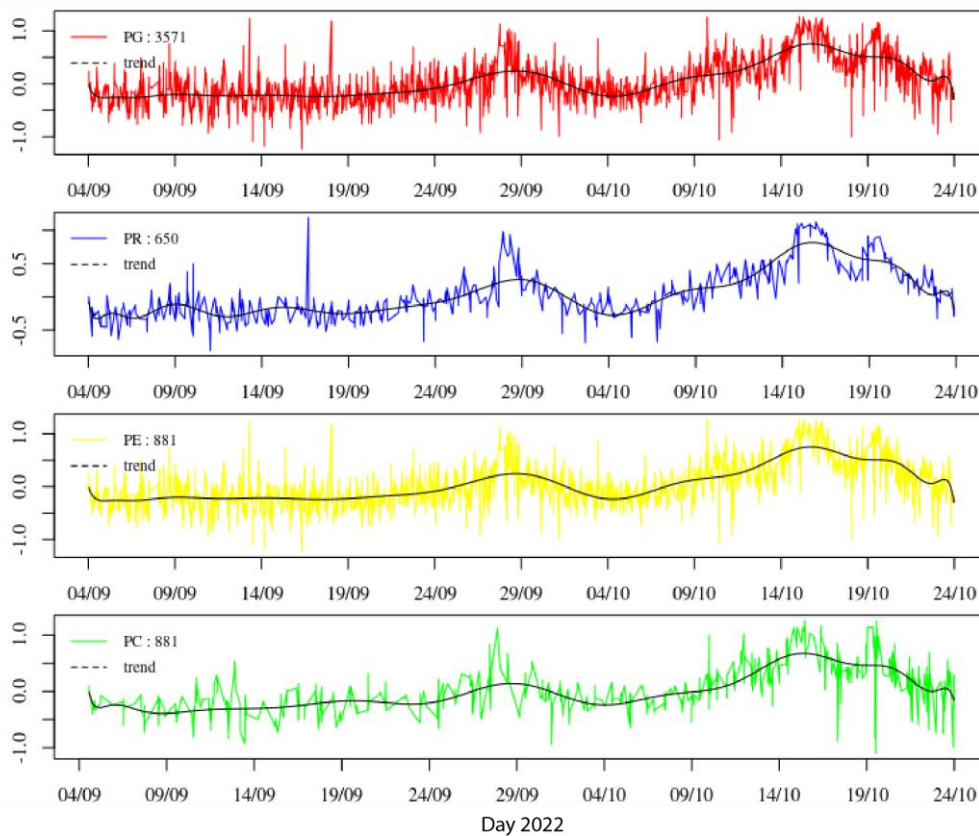


Fig. 6. The GNSS-R SSH in Tam Giang lagoon, Thua Thien Hue, from September 4 to October 24, 2022. a) GPS (PG), b) GLONASS (PR), c) Galileo (PE) and d) BeiDou (PC).

Case study: Storm Noru 26–28 September 2022, and the flood from October 14-19, 2022

The results of the SSA analysis were performed on the GNSS-R data collected at Tam Giang station. The GNSS-R-based water level time series is decomposed into four major components: $RC_1=82.11\%$, $RC_2=5.48\%$, $RC_3 = 5.1\%$, and $RC_4 = 1.48\%$ (Fig. 7). The PC2 and PC3 components correspond to the tidal signals in the GNSS-R data, while the PC1 component represents low-frequency signal in the sea level data.

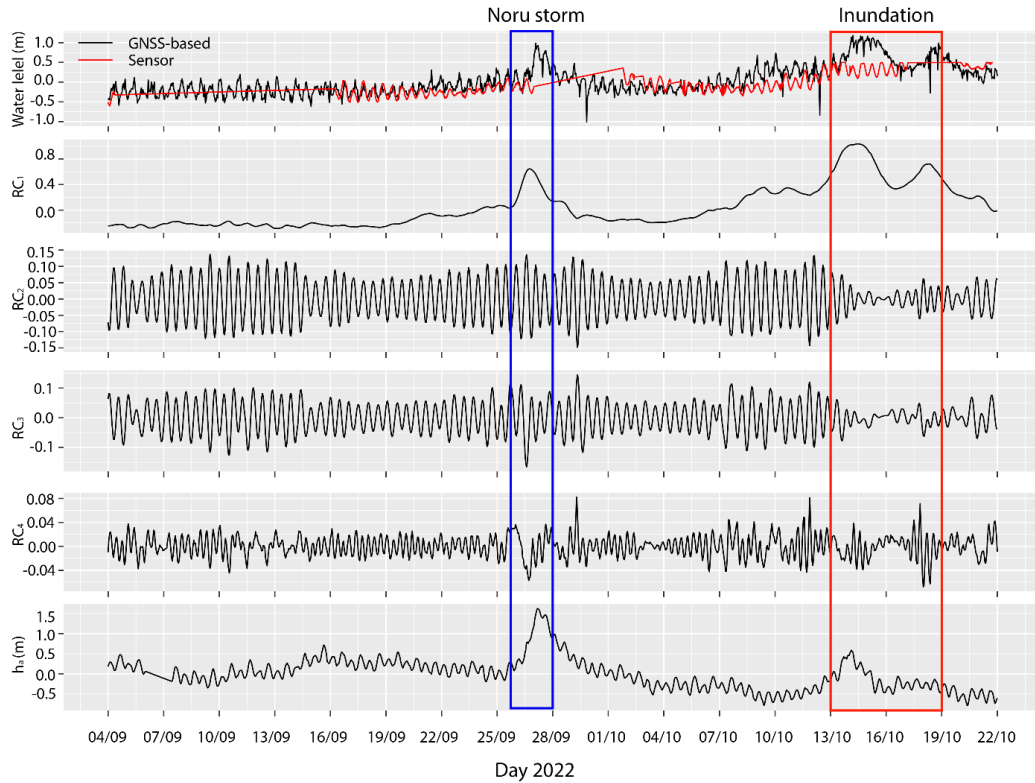


Fig. 7. Water height GNSS-based and the four main components of its SSA decomposition and atmospheric data

The RC4 component represents the freshwater input from the O Lau River and some other signals such as waves, wind...By decomposing the sea level time series into its major components, SSA makes it possible to isolate the specific signals associated with the typhoon, such as changes in sea level due to tidal effects, wind-driven waves, or other meteorological factors. This analysis has revealed distinct signatures in the data corresponding to the Noru typhoon that occurred from September 27-28, 2022, and the flood that occurred from October 14-19, 2022.

The signs and timing of the Noru Typhoon are clearly shown through cross-correlation analysis (XWT) between GNSS-R SSH data and water level change due to the influence of barometric pressure. The results in Figure 8 show a strong correlation between tides and water levels based on GNSS-R at a 0.5-day period, but there are no significant differences between the two data sets during the storm period. However, in the period from 1 day to 8 days, there is a high correlation between the two data series during the Noru Typhoon.

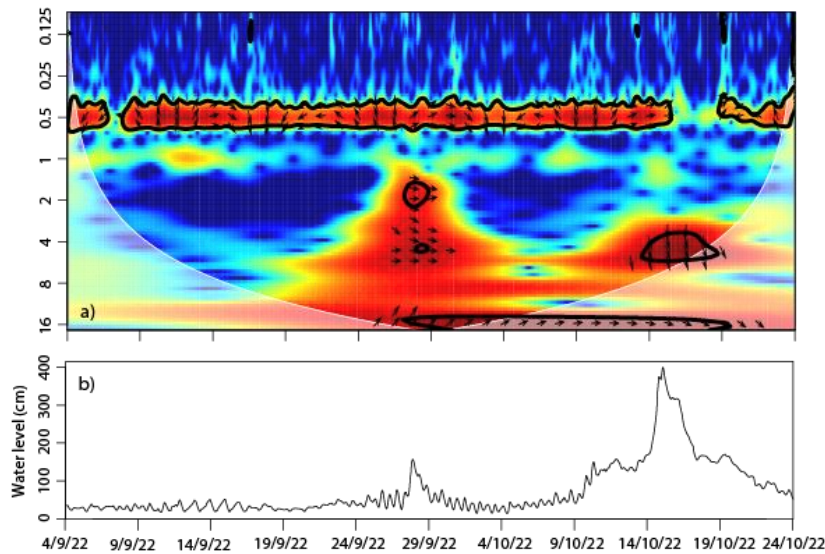


Fig. 8. a) XWT between GNSS-R SSH and water level change due to the influence of barometric pressure (h_a); b) The water level was measured at the Kim Long hydrological station, about 15 km from the GNSS station

This can be explained by the sharp drop in pressure near the center of the storm, causing the water level to rise. The direction of the arrows in the XWT plots represents the phase relationship between two-time series at a given frequency and period. Arrows indicate the in-phase (pointing right) during the Noru Typhoon, showing a positive correlation between the two GNSS-R SSH data and water level changes due to barometric pressure. That proves both data are affected by atmospheric pressure, causing waves and strong winds. However, during flooding due to heavy rain in the mountainous area of XX at the end of October (October 14-19), the GNSS-R signal had an opposite phase between meteorological data series, although there is also a very high correlation. The water level was mainly influenced by the amount of rainfall and the flow of water from upstream. In addition, the observed period for the occurrence of flooding is also longer (within a period of 4-8 days). Comparing the two extreme hydrological events occurring in the GNSS-R SSH data series, we can see the difference in water levels between the two events above. For Typhoon Noru, the water level was significantly influenced by barometric pressure and wind waves, and the answer to this phenomenon on the sea surface is immediate. In contrast, during the flood at the end of October, the water level is greatly influenced by the amount of rain and water from the O Lau River, and the needed transit time of the water introduces a delay between meteorological data and GNSS-R observations.

Discussion

This study shows that the low-cost antenna can measure water levels and extract tides with the same accuracy as a standard geodetic antenna, even in harsh coastal environments. However, their performance can vary depending on several factors. The accuracy of these receivers can be affected by the number and distribution of satellites, atmospheric conditions, and signal obstructions. Under specific conditions, it is possible to combine multiple low-cost antennas to increase the accuracy of the measurement results (Purnell, Gomez, & Minarik, 2020; David J. Purnell, 2021; Chenyu Xue, 2022). In the study, low-cost antennas demonstrated superior advantages over standard geodetic antennas in determining the occurrence of extreme hydrological events. This can be explained by the fact that the standard antenna is designed to reduce the multipath interference present in the measurement results. Meanwhile, low-cost antennas can pick up more multipath signals – necessary data for estimating water levels and determining storm surges using GNSS-R signals (Phuong Lan Vu et al., 2019; Dongju Peng, 2019; Gravalon, Seoane, Darrozes, & Ramillien, 2021). On the other hand, low-cost GNSS receivers consume less power than high-precision receivers, making them suitable for remote and battery-operated applications. Additionally, low-cost GNSS receivers are small, lightweight, and can be easily deployed for temporary or mobile monitoring applications. By combining GNSS data with other environmental sensors, such as wind, pressure, and wave height sensors, low-cost GNSS receivers can provide valuable information for storm detection and response. Once the typhoon signature has been isolated in the GNSS-R data, further analysis can be performed to quantify the magnitude and duration of the storm surge, wind-driven waves, and other meteorological effects associated with the typhoon. This information can be used to improve the accuracy of predictive models and to inform disaster response and management efforts.

Many studies have developed GNSS-R technology applications from CYGNSS data to retrieve soil moisture (Yifan Zhu, 2022; Sizhe Chen, 2022; Minh Cuong Ha et al., 2022), establish dynamic flood mapping (P. Zeiger, 2022; Huu Duy Nguyen, 2022), and hurricane research (Lucrezia Ricciardulli, 2021). The data obtained from low-cost GNSS stations can be combined with CYGNSS data to monitor floods and droughts by measuring changes in soil moisture and surface water levels. Integrating data from these stations and CYGNSS data can improve storm forecasting and enable more accurate storm tracking.

Conclusions

This study demonstrated the performance of low-cost GNSS receivers for tidal monitoring and detecting extreme events. The water level results obtained from GNSS-R data were collected at a GNSS station located in the Tam Giang Lagoon area, Thua Thien Hue, Vietnam, from September to October 2022 and compared with the water level measured by the sensor, yielding a correlation coefficient of 0.96 and an RMSE of 0.08m. Singular spectrum analysis and continuous wavelet analysis were employed to decompose the SSH GNSS-R signal. The results revealed distinct signatures in the data that corresponded to the occurrence of the Noru typhoon from September 27 to 28, 2022, and the inundation that occurred from October 14 to 19, 2022. This information serves as the basis for forecasting and early warning of extreme events and informing disaster response and management efforts.

References

- Arjumand Z. Zaidi et al. (2021). Indus river water level monitoring using satellite radar altimetry. *Advances in Space Research*.
- Ben Clarke, F. O.-S. (2022). Extreme weather impacts of climate change: an attribution perspective. *Environmental Research: Climate*.
- Box, G., & Jenkins, G. (1970). Time Series Analysis: Forecasting and Control. *Wiley Series in Probability and Statistics*.
- Brief, C. (2022). *Mapped: How climate change affects extreme weather around the world*.
- Cazenave, A. (2018). Global sea-level budget 1993–present. *Earth Syst. Sci. Data*, 10, 1551–1590.
- Cazenave, R. J. (2010). Sea-Level Rise and Its Impact on Coastal Zones. *Science*.
- Charls Antony, L. T. (2014). Observing storm surges in the Bay of Bengal from satellite altimetry. *Estuarine, Coastal and Shelf Science*.
- Chenyu Xue, X. M. (2022). Feasibility analysis of the performance of low-cost GNSS receivers in monitoring dynamic motion. *Measurement*.
- Crétaux, J.-F. e. (2017). Hydrological applications of satellite altimetry: rivers, lakes, man-made reservoirs, inundated areas. Dans *In Satellite Altimetry Over Oceans and Land Surfaces* (pp. 459-504). Earth Observation of Global Changes.
- D. Purnell et al. (2020). Quantifying the Uncertainty in Ground-Based GNSS Reflectometry Sea Level Measurements. *IEEE Journal of Selected Topics in Applied Earth Observations and Remote Sensing*, 4419-4428.
- David J. Purnell, N. G. (2021). Precise water level measurements using low-cost GNSS antenna. *Earth Surface Dynamics*.
- Dongju Peng, E. M. (2019). Application of GNSS interferometric reflectometry for detecting storm surges. *GPS Solutions*.
- Duc Thanh Tran et al. (2022, 05 10). *Thua Thien Hue Portal*. Récupéré sur General Characteristics of The Tam Giang – Cau Hai Lagoon System: <https://thuathienhue.gov.vn/vi-vn/Thong-tin-du-dia-chi/tid/>
- Frédéric Frappart, N. R. (2016). High rate GNSS measurements for detecting non-hydrostatic surface wave. Application to tidal bore in the Garonne River. *European Journal of Remote Sensing*.
- Gravalon, T., Seoane, L., Darrozes, J., & Ramillien, G. (2021). The Impact of Barometric Variations on the Sea Level in Coastal Areas Using GNSS Reflectometry. *IEEE International Symposium on Geoscience and Remote Sensing (IGARSS)*. IEEE.
- Haas, J. S. (2014). Sea level measurements using multi-frequency GPS and GLONASS observations. *EURASIP Journal on Advances in Signal Processing*.
- Heiko Apel, H. N. (2012). GPS buoys for stage monitoring of large rivers. *Journal of Hydrology*.
- Huu Duy Nguyen, P. L. (2022). Flood susceptibility mapping using advanced hybrid machine learning and CyGNSS: a case study of Nghe An province, Vietnam. *Acta Geophysica*.
- J. Beckheinrich et al. (2014). Water Level Monitoring of the Mekong Delta Using GNSS Reflectometry Technique. *IEEE Geoscience and Remote Sensing Symposium*.
- J. S. Löfgren, R. H. (2011). Three Months of Local Sea Level Derived From Reflected GnsS Signals. *Radio Science*, 46(6), 1-12.
- Jérôme Benveniste et al. (2019). Requirements for a Coastal Hazards Observing System. *Front. Mar. Sci.*.
- Jieying Lao, C. W. (2022). Monitoring and Analysis of Water Level Changes in Mekong River from ICESat-2 Spaceborne Laser Altimetry. *Water*.
- Jonathan M. Frame, F. K. (2022). Deep learning rainfall–runoff predictions of extreme events. *Hydrol. Earth Syst. Sci.*
- K. M. Larson et al. (2020). Dynamic Sea Level Variation From GNSS: 2020 Shumagin Earthquake Tsunami Resonance and Hurricane Laura. *Geophysical Research Letters*.
- Kaitano Dube, G. N. (2022). Flooding trends and their impacts on coastal communities of Western Cape Province, South Africa. *GeoJournal*, 453-468.
- Kovanič, E.; Blistan, P.; Štroner, M.; Urban, R.; Blistanova, M. Suitability of Aerial Photogrammetry for Dump Documentation and Volume Determination in Large Areas. *Appl. Sci.* **2021**, 11, 6564.
- Kovanič, L.; Blistan, P.; Rozložník, M.; Szabó, G. UAS RTK/PPK photogrammetry as a tool for mapping the urbanized landscape, creating thematic maps, situation plans and DEM. *Acta Montan. Slovaca* **2022**, 26, 649–660
- Kovanič, E.; Štroner, M.; Urban, R.; Blišťan, P. (2023)a Methodology and Results of Staged UAS Photogrammetric Rockslide Monitoring in the Alpine Terrain in High Tatras, Slovakia, after the Hydrological Event in 2022. *Land* **2023**, 12, 977. <https://doi.org/10.3390/land12050977>

- Kovanič, L.; Topitzer, B.; Peřovský, P.; Blišťan, P.; Gergelřová, M.B.; Blišťanová, M. (2023)b. Review of Photogrammetric and Lidar Applications of UAV. *Appl. Sci.* **2023**, *13*, 6732
- Kovanič, L.; Peřovský, P.; Topitzer, B.; Blišťan, P. Complex Methodology for Spatial Documentation of Geomorphological Changes and Geohazards in the Alpine Environment. *Land* **2024**, *13*, 112. <https://doi.org/10.3390/land13010112>
- Kristine M. Larson, E. E. (2008). Using GPS Multipath to Measure Soil Moisture Fluctuations: Initial Results. *GPS Solutions*.
- Lucrezia Ricciardulli, C. M. (2021). Assessment of CYGNSS Wind Speed Retrievals in Tropical Cyclones. *Remote sensing*.
- Lukas Gudmundsson et al, .. (2021). Globally observed trends in mean and extreme river flow attributed to climate change. *Science*, 1159-1162.
- M. A. R. Fagundes, I. M.-T.-N. (2021). An open-source low-cost sensor for SNR-based GNSS reflectometry: design and long-term validation towards sea-level altimetry. *GPS Solutions*.
- Malhi GS, K. M. (2021). Impact of climate change on agriculture and its mitigation strategies: a review. . *Sustainability*.
- Minh Cuong Ha et al. (2022). GNSS-R monitoring of soil moisture dynamics in areas of severe drought: example of Dahra in the Sahelian climatic zone (Senegal). *European Journal of Remote Sensing* .
- Mohammad Kazemi Garajeh, B. S. (2023). An integrated approach of remote sensing and geospatial analysis for modeling and predicting the impacts of climate change on food security. *Scientific Reports*.
- N. Roussel et al. (2015). Sea Level Monitoring And Sea State Estimate Using A Single Geodetic Receiver . *Remote Sensing of Environment*.
- N. Roussel, F. F. (2014). Simulations of direct and reflected waves trajectories for in situ GNSS-R experiments. *Geosci. Model Dev. Discuss*.
- Nicolas Roussel, G. R. (2015). Sea level monitoring and sea state estimate using a single geodetic receiver. *Remote sensing of Environment*, 261-277.
- Ole B. Andersen, Y. C. (2015). Using satellite altimetry and tide gauges for storm surge warning. *Proceedings of HP2/HP3*. Gothenburg, Sweden: IAHS-IAPSO-IASPEI Assembly.
- P. Zeiger, F. F. (2022). Introducing the global mapping of flood dynamics using GNSS-Reflectometry and the cygnss mission. *ISPRS Annals of the Photogrammetry, Remote Sensing and Spatial Information Sciences*.
- Phuong Lan Vu et al, .. (2018). Multi-Satellite Altimeter Validation along the French Atlantic Coast in the Southern Bay of Biscay from ERS-2 to SARAL. *Remote sensing*.
- Phuong Lan Vu et al. (2019). Identifying 2010 Xynthia Storm Signature in GNSS-R-Based Tide Records. *Remote Sensing* .
- Phuong Lan, V. e. (2022). Application of GNSS Reflectometry in Water Level Monitoring using Low-cost GNSS Antenna: A Case Study in Tam Giang Lagoon, Thua Thien Hue Province. *VNU Journal of Science: Earth and Environmental Sciences*.
- Ponte, R. M. (2006). Low-frequency sea level variability and the inverted barometer effect. *J. Atmos. Oceanic Technol.*
- Prashant Kumar et al. (2021). An overview of monitoring methods for assessing the performance of nature-based solutions against natural hazards. *Earth-Science Reviews*.
- Purnell, D., Gomez, N. A., & Minarik, W. G. (2020). Precise water level measurements using multiple low-cost GNSS antennas. *American Geophysical Union*.
- R.Vautard and M.Ghil, .. (1989). Singular spectrum analysis in nonlinear dynamics, with applications to paleoclimatic time series. *Physica D: Nonlinear Phenomena*.
- S Jonas, K. F. (2018). A framework to understand extreme space weather event probability. *Risk Analysis*.
- S. Biancamaria et al. (2017). Satellite radar altimetry water elevations performance over a hundred meter wide river: evaluation over the Garonne River. *Advances in Space Research*.
- Seneviratne, S. X.-S. (2021). Weather and Climate Extreme Events in a Changing Climate. Dans *Climate Change 2021: The Physical Science Basis* .
- Sizhe Chen, Q. Y. (2022). Soil Moisture Retrieval from the CyGNSS Data Based on a Bilinear Regression. *Remote Sensing*.
- Su-Kyung Kim et al, .. (2021a). Monitoring a storm surge during Hurricane Harvey using multi-constellation GNSS-Reflectometry. *GPS Solutions*.
- Su-Kyung Kim, E. L. (2021b). Feasibility Analysis of GNSS-Reflectometry for Monitoring Coastal Hazards. *Remote Sensing*.
- Tabari, V. O. (2022). Climate Impacts on Extreme Weather, Current to Future Changes on a Local to Global Scale. Dans *Climate Impacts on Extreme Weather*.
- Tao Ji, G. Y. (2019). Observing storm surges in China's coastal areas by integrating multi-source satellite altimeters. *Estuarine, Coastal and Shelf Science*.

- Tasneem Ahmed, L. C. (2023). Low-Cost Sensors for Monitoring Coastal Climate Hazards: A Systematic Review and Meta-Analysis. *sensors*.
- Torrence, C., & Compo, G. A. (1998). Practical Guide to Wavelet Analysis. *Am. Meteorol. Soc.* .
- Vousdoukas, M., Mentaschi, L., Voukouvalas, E., Verlaan, M., Jevrejeva, S., Jackson, L., & Feyen, L. (2018). Global probabilistic projections of extreme sea levels show intensification of coastal flood hazard. *Nat. Commun.*
- Wentao Yang, F. G. (2021). Daily Flood Monitoring Based on Spaceborne GNSS-R Data: A Case Study on Henan, China. *Remote sensing*.
- World Meteorological Organization. (2021). *Weather-related disasters increase over past 50 years, causing more damage but fewer deaths*. Récupéré sur WORLD METEOROLOGICAL ORGANIZATION: <https://public.wmo.int/en/media/press-release/weather-related-disasters-increase-over-past-50-years-causing-more-damage-fewer>
- Xiaohui Li et al, .. (2021). Exploiting the Potential of Coastal GNSS-R for Improving Storm Surge Modeling. *IEEE Geoscience and Remote Sensing Letters*.
- Xiaohui Li, G. H. (2018). Using Satellite Altimetry to Calibrate the Simulation of Typhoon Seth Storm Surge off Southeast China. *Remote Sensing*.
- Xiaolei Wang, X. H. (2021). Millimeter to centimeter scale precision water-level monitoring using GNSS reflectometry: Application to the South-to-North Water Diversion Project, China. *Remote Sensing of Environment*.
- Yifan Zhu, F. G. (2022). Effect of surface temperature on soil moisture retrieval using CYGNSS. *International Journal of Applied Earth Observation and Geoinformation*.
- Zhou Qiu, G. Z. (2019). Jason-1 Observation of Typhoon Storm Surge and Analysis Based on Numerical Simulation. *IOP Conference Series: Materials Science and Engineering*.
- In-text reference:* (Pickett and McDonnell, 2017)